

Numerical Simulations of Hydrodynamics with Lattice Gas Automata in Two Dimensions

Dominique d'Humières
Pierre Lallemand

*CNRS, Laboratoire de Physique de l'Ecole Normale Supérieure,
24 rue Lhomond, 75231 Paris Cedex 05, France*

Abstract. We present results of numerical simulations of the Frisch, Hasslacher, and Pomeau lattice gas model and of some of its variants. Equilibrium distributions and several linear and nonlinear hydrodynamics flows are presented. We show that interesting phenomena can be studied with this class of models, even for lattices of limited sizes.

1. Introduction

Since Frisch, Hasslacher, and Pomeau [1] have shown that particles moving on a triangular lattice with very simple collisions on the nodes of the lattice obey the Navier-Stokes equation, the use of lattice gas models to study hydrodynamics has received considerable interest during the last two years [2]. However, the Navier-Stokes equation is recovered only in the limit of large systems and for incompressible flows. More theoretical analysis remains to be done to bound the errors of the lattice gas numerical scheme for finite lattice sizes and velocities. At present, some partial answers to this question can be obtained by numerical simulations of the dynamical behavior of the triangular lattice gases and by comparison of these results with classical hydrodynamics.

In section 2, we will describe precisely the models we have studied and recall briefly their theoretical properties obtained with the Boltzmann approximation [2,3]. Section 3 will be devoted to a detailed description of how these models can be simulated on general-purpose computers. In section 4, numerical evidence of the Fermi-Dirac distribution for equilibrium will be presented. The measurement of the transport coefficients will be given in section 5. Finally, we will report in section 6 some examples of nonlinear flows either for stationary or nonstationary situations for moderate Reynolds numbers.

2. The models

We consider particles moving on a triangular lattice with unit velocity \mathbf{c}_i in direction i between a node and one of its six neighbors ($i = 1, \dots, 6$). At each time step, particles incoming on a node interact together according to collision laws assumed to conserve the number of particles and the total linear momentum on the node. The particles then propagate according to their new velocity. In addition, there is an exclusion principle such that no two particles with the same velocity may occupy the same node at the same time (0 or 1 particle per cell, as defined in reference 2). Thus, each node of the lattice can be described by a six-bit word whose ones represent particles moving with the velocities associated with their bit positions within the word.

We have also used variants of these six-bit models which allow additional particles with zero velocity at each site ($i = 0$ for notational purposes). Thus, we can introduce seven-bit models with at most one "rest particle" per lattice node, or eight-bit models with up to three rest particles per node.¹ In the eight-bit models, two bits are used to code the presence of rest particles, one for mass-one particles and one for a new kind of rest particle of mass two, equivalent to two rest particles of mass one. To handle the case of particles with zero velocity and different masses, the theoretical results of reference 2 need some modifications, given in Appendix A. Here, we will give the general results for the case of b_m moving particles with unit mass and b_r rest particles with mass $m_k = 2^k$, $k \in \{0, \dots, b_r - 1\}$. The macroscopic quantities: density ρ and momentum $\rho \mathbf{u}$, are related to the local average populations N_{ik} of particles with mass 2^k and velocity \mathbf{c}_i , by

$$\rho = \sum_{i,k} 2^k N_{ik}; \quad \rho \mathbf{u} = \sum_{i,k} 2^k N_{ik} \mathbf{c}_i. \quad (2.1)$$

These populations are given by the following Fermi-Dirac distributions

$$N_{ik} = \frac{1}{1 + \exp(2^k(h + \mathbf{q} \cdot \mathbf{c}_i))} \quad (2.2)$$

where h and \mathbf{q} are nonlinear functions of ρ and \mathbf{u} . When $\mathbf{u} = 0$, the average density is the same for all the particles with same mass 2^k and will be denoted d_k ; taking the mass of the lightest particles as unit mass and $d_0 = d$, one gets

$$d_k = \frac{d^{2^k}}{d^{2^k} + (1 - d)^{2^k}} \quad (2.3)$$

Thus, when particles with mass greater than one are added, the density is related by a nonlinear law to the average density of particles of mass one,

¹These particles may be considered to have an internal energy to satisfy energy conservation which is undistinguishable from mass conservation.

which will be called “density per cell” in what follows, as was done for the case where all the particles have the same mass. This nonlinear relation implies that all the expansions around equilibrium cannot take the simple expressions used in reference 2. The density of moving and rest particles, ρ_m and ρ_r respectively, can be defined as

$$\rho_m = b_m d \quad \text{and} \quad \rho_r = \sum_{k=0}^{b_r-1} 2^k d_k, \quad \text{with} \quad \rho = \rho_m + \rho_r; \quad (2.4)$$

For small u , the expansion of (2.2) up to first order gives

$$\begin{aligned} N_{i0}^{eq} &= d \left(1 + \frac{2\rho}{\rho_m} \mathbf{c}_i \cdot \mathbf{u} \right), \\ N_{0k}^{eq} &= d_k. \end{aligned} \quad (2.5)$$

The speed of sound is given by

$$c_s^2 = \frac{b_m d(1-d)}{2(b_m d(1-d) + \sum_{k=0}^{b_r-1} 4^k d_k(1-d_k))} \quad (2.6)$$

and, up to second-order terms in velocity and gradients, the lattice gas dynamics is described by²

$$\begin{aligned} \partial_t \rho + \operatorname{div}(\rho \mathbf{u}) &= 0 \\ \partial_t(\rho u_\alpha) + \partial_\beta(g(\rho) \rho u_\alpha u_\beta) &= \\ \partial_\alpha P(\rho, u^2) + \partial_\beta(\nu \partial_\beta(\rho u_\alpha)) + \partial_\alpha(\zeta \operatorname{div}(\rho \mathbf{u})) & \end{aligned} \quad (2.7)$$

with

$$\begin{aligned} g(\rho) &= \frac{\rho}{2\rho_m} \frac{1-2d}{1-d}, \quad P(\rho, u^2) = \frac{\rho_m}{2} - \frac{\rho}{2} g(\rho) (4c_s^2 - 1) u^2, \\ \text{and } \nu &= -\frac{1}{4\lambda} - \frac{1}{8} \end{aligned} \quad (2.8)$$

where the kinematic shear viscosity ν is related to the eigenvalue λ of the linearized collision matrix $[A_{IJ}]$ corresponding to the eigenvector $[c_{ix} c_{iy}]$, and the kinematic bulk viscosity ζ is related in a complicated way to $[A_{IJ}]$, as shown in Appendix A.³

²Greek and Roman indices refer respectively to components, and velocity labels and the summations over repeated Greek indices are implicit.

³Capital Roman indices I and J refer to double lowercase roman indices ik and jl .

2.1 Six-bit model: model I

Table 1 gives all the possible configurations of the six-bit models, listing only the cases such that $j_x \geq j_y \geq 0$ [4]. The first three columns give the number of particles and the total momentum.⁴ The fourth column shows the different configurations, the legal collisions exchanging configurations appearing within the same row, and the last column gives the number of different configurations obtained by the application of the symmetry group. To avoid bit representation of the collision probabilities $A(s \rightarrow s')$ between states $sands'$, we have chosen to write this probability $A_I(j \rightarrow k)$, where I is an index representing the number of particles, and the total momentum as it is given in the three first columns of table 1 and j and k are the positions of configurations in the rows of this table. The legal collision rules exclude the exchange of configurations belonging to different rows of the configuration table, and in the case of only one configuration, $A_I(1 \rightarrow 1) = 1$. With this notation, the semi-detailed balance is written:

$$\sum_j A_I(j \rightarrow k) = \sum_k A_I(j \rightarrow k) = 1 \quad \forall I$$

The original FHP (model I) model uses only the collision rules exchanging the configurations within rows 3 and 6:

$$A_I(j \rightarrow k) = \delta_{jk} \quad \forall I \neq \{200, 300\};$$

$$A_{200}(j \rightarrow k) = \frac{1 - \delta_{jk}}{2} \quad j, k \in \{1, 2, 3\};$$

$$A_{300}(j \rightarrow k) = 1 - \delta_{jk} \quad j, k \in \{1, 2\}.$$

These collision rules: three two-body head-on collisions and two symmetric three-body collisions, changes five configurations among the 64 possible ones. They are the minimal set of rules to prevent spurious conservation laws.

For this model, the transport coefficients are given by

$$\rho = \rho_m = 6d, \quad c_s = \frac{1}{\sqrt{2}},$$

$$g(\rho) = (\rho - 3)/(\rho - 6), \quad P = \frac{\rho}{2}(1 - g(\rho)u^2) \quad (2.9)$$

$$\nu = \frac{1}{12d(1 - d)^3} - \frac{1}{8}, \quad \zeta = 0 \quad (2.10)$$

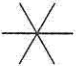





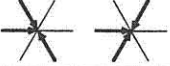
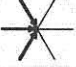





| n | j_x | j_y | | folds |
|---|-------|-------|---|-------|
| 0 | 0 | 0 |  | 1 |
| 1 | 2 | 0 |  | 6 |
| 2 | 0 | 0 |  | 1 |
| 2 | 2 | 0 |  | 6 |
| 2 | 3 | 2 |  | 6 |
| 3 | 0 | 0 |  | 1 |
| 3 | 2 | 0 |  | 6 |
| 3 | 4 | 0 |  | 6 |
| 4 | 3 | 2 |  | 6 |
| 4 | 2 | 0 |  | 6 |
| 4 | 0 | 0 |  | 1 |
| 5 | 2 | 0 |  | 6 |
| 6 | 0 | 0 |  | 1 |

Table 1: List of configurations for the six-bit FHP model. Column 1 gives the number of particles, column 2 gives $2j_x$, column 3 gives $4j_y/\sqrt{3}$, and the last column gives the number of equivalent collisions that can be obtained by successive $\frac{\pi}{3}$ rotations when "fold" $\neq 1$.




















| n | jx | jy | | folds |
|---|----|----|---|-------|
| 0 | 0 | 0 |  | 1 |
| 1 | 0 | 0 |  | 1 |
| 1 | 2 | 0 |  | 6 |
| 2 | 0 | 0 |    | 1 |
| 2 | 2 | 0 |   | 6 |
| 2 | 3 | 2 |  | 6 |
| 3 | 0 | 0 |      | 1 |
| 3 | 2 | 0 |    | 6 |
| 3 | 3 | 2 |  | 6 |
| 3 | 4 | 0 |  | 6 |

Table 2: List of configurations for the seven-bit models. Configurations with four particles and more are obtained by duality replacing particles by holes and holes by particles.

2.2 Seven-bit models: models II and III

Actually, most of the computer simulations were done with the model that includes rest particles. Table 2 lists all the configurations up to three particles; the configurations for more than three particles are obtained by duality (exchange of particles and holes) from the listed configurations. For the seven-bit models, the "universal" transport coefficients are given by

$$\rho = 7d, \quad \rho_m = 6d, \quad c_s = \sqrt{\frac{3}{7}},$$

$$g(\rho) = \frac{7}{12} \frac{7-2\rho}{7-\rho}, \quad P = \frac{3\rho}{7} \left(1 - \frac{5}{6} g(\rho) u^2\right) \quad (2.11)$$

Model II is defined by the following collision rules:

$$A_I(j \rightarrow k) = \delta_{jk} \quad \forall I \neq \{200, 2_{20}^{\leftarrow}, 300, 400\};$$

$$A_{200}(j \rightarrow k) = \frac{1 - \delta_{jk}}{2} \quad j, k \in \{1, 2, 3\};$$

$$A_{2_{20}^{\leftarrow}}(j \rightarrow k) = 1 - \delta_{jk} \quad j, k \in \{1, 2\};$$

$$A_{300}(j \rightarrow k) = \frac{1 - \delta_{jk}}{2} \quad j, k \in \{1, 2, 3\};$$

$$A_{400}(j \rightarrow k) = 1 - \delta_{jk} \quad j, k \in \{4, 5\};$$

$$A_{300}(j \rightarrow k) = A_{300}(k \rightarrow j) = 0 \quad j \in \{1, 2, 3\} \quad k \in \{4, 5\};$$

$$A_{400}(j \rightarrow k) = \delta_{jk} \quad j, k \in \{1, 2, 3\};$$

$$A_{400}(j \rightarrow k) = 1 - \delta_{jk} \quad j, k \in \{4, 5\};$$

$$A_{400}(j \rightarrow k) = A_{400}(k \rightarrow j) = 0 \quad j \in \{1, 2, 3\} \quad k \in \{4, 5\};$$

representing 22 configurations giving active collisions: ten identical to model I with or without rest particles as "spectator" plus twelve two-body collisions changing the number of rest particles. The viscosities are given by

$$\nu = \frac{1}{28d(1-d)^3(1-4d/7)} - \frac{1}{8}, \quad \zeta = \frac{1}{98d(1-d)^4} - \frac{1}{28} \quad (2.12)$$

Model III is defined using effective collision rules for all the possible configurations, with the following rules:

⁴To use only integers, j_x is multiplied by two and j_y by $4/\sqrt{3}$. Starting from momentum $(2, 0)$, successive $\frac{\pi}{3}$ rotations give $(1, 2)$, $(-1, 2)$, $(-2, 0)$, $(-1, -2)$, and $(1, -2)$. In this paper, such sets of configurations with p particles will be denoted p_{20}^{\leftarrow} .

$$A_I(1 \rightarrow 1) = 1 \quad \forall I \text{ such that } q_I = 1;$$

$$A_I(j \rightarrow k) = \frac{1 - \delta_{jk}}{q_I - 1} \quad \forall I \text{ such that } 1 < q_I < 4, j, k \in \{1, \dots, q_I\};$$

$$A_{300}(j \rightarrow k) = \frac{1 - \delta_{jk}}{2} j, k \in \{1, 2, 3\}; A_{300}(j \rightarrow k) = 1 - \delta_{jk} j, k \in \{4, 5\};$$

$$A_{300}(j \rightarrow k) = A_{300}(k \rightarrow j) = 0 \quad j \in \{1, 2, 3\} \quad k \in \{4, 5\};$$

$$A_{400}(j \rightarrow k) = \frac{1 - \delta_{jk}}{2} j, k \in \{1, 2, 3\}; A_{400}(j \rightarrow k) = 1 - \delta_{jk} j, k \in \{4, 5\};$$

$$A_{400}(j \rightarrow k) = A_{400}(k \rightarrow j) = 0 \quad j \in \{1, 2, 3\} \quad k \in \{4, 5\};$$

where q_I is the number of configurations in the I^{th} row of table 2. With these rules, which are self-dual, 76 configurations give active collisions. The viscosities are given by

$$\begin{aligned} \nu &= \frac{1}{28d(1-d)(1-8d(1-d)/7)} - \frac{1}{8}, \\ \zeta &= \frac{1}{98d(1-d)(1-2d(1-d))} - \frac{1}{28}. \end{aligned} \quad (2.13)$$

2.3 Eight-bit model: model IV

We also used a model with rest particles of mass two in addition to the seven particles used in models II and III. Table 2 lists all the configurations up to four particles; the configurations for more than four particles can be obtained taking the dual of the listed configurations. For the eight-bit models, the "universal" transport coefficients are given by

$$\begin{aligned} \rho &= d\left(7 + \frac{2d}{d^2 + (1-d)^2}\right), \quad \rho_m = 6d, \\ c_s &= \sqrt{\frac{3(d^2 + (1-d)^2)^2}{7(d^2 + (1-d)^2)^2 + 4d(1-d)}}, \\ g(\rho) &= \frac{1}{12}\left(7 + \frac{2d}{d^2 + (1-d)^2}\right)\frac{1-2d}{1-d}, \\ P &= 3d - \frac{\rho}{2}g(\rho)\left(\frac{5(d^2 + (1-d)^2)^2 - 4d(1-d)}{7(d^2 + (1-d)^2)^2 + 4d(1-d)}\right)u^2. \end{aligned} \quad (2.14)$$

Model IV is defined by the following collision rules:

$$A_I(j \rightarrow k) = \delta_{jk} \quad \forall I \neq \{200, 2_{20}^{\leftarrow}, 300, 3_{20}^{\leftarrow}, 400, 4_{20}^{\leftarrow}, 500, 600\};$$

$$A_{200}(1 \rightarrow 1) = 1; \quad A_{200}(j \rightarrow k) = \frac{1 - \delta_{jk}}{2};$$

$$j, k \in \{2, 3, 4\}; \quad A_{200}(1 \rightarrow j) = 0 \quad j \in \{2, 3, 4\};$$

$$A_{220}(j \rightarrow k) = 1 - \delta_{jk} \quad j, k \in \{1, 2\};$$

$$A_{300}(1 \rightarrow 1) = 1; \quad A_{300}(j \rightarrow k) = \frac{1 - \delta_{jk}}{2} \quad j, k \in \{2, 3, 4\};$$

$$A_{300}(j \rightarrow k) = 1 - \delta_{jk} \quad j, k \in \{5, 6\};$$

$$A_{300}(1 \rightarrow j) = 0 \quad j \in \{2, 3, 4, 5, 6\};$$

$$A_{300}(j \rightarrow k) = A_{300}(k \rightarrow j) = 0 \quad j \in \{2, 3, 4\} \quad k \in \{5, 6\};$$

$$A_{320}(j \rightarrow k) = 1 - \delta_{jk} \quad j, k \in \{1, 2\};$$

$$A_{320}(j \rightarrow k) = \delta_{jk} \quad j, k \in \{3, 4\};$$

$$A_{320}(j \rightarrow k) = A_{320}(k \rightarrow j) = 0 \quad j \in \{1, 2\} \quad k \in \{3, 4\};$$

$$A_{400}(j \rightarrow k) = \frac{1 - \delta_{jk}}{2} \quad j, k \in \{1, 2, 3\};$$

$$A_{400}(j \rightarrow k) = 1 - \delta_{jk} \quad j, k \in \{4, 5\};$$

$$A_{400}(j \rightarrow k) = \delta_{jk} \quad j, k \in \{6, 7, 8\};$$

$$A_{400}(j \rightarrow k) = A_{400}(k \rightarrow j) = 0$$

$$j \in \{1, 2, 3\} \quad k \in \{4, 5, 6, 7, 8\};$$

$$A_{400}(j \rightarrow k) = A_{400}(k \rightarrow j) = 0 \quad j \in \{4, 5\} \quad k \in \{6, 7, 8\};$$

$$A_{420}(j \rightarrow k) = 1 - \delta_{jk} \quad j, k \in \{1, 2\};$$

$$A_{420}(j \rightarrow k) = \delta_{jk} \quad j, k \in \{3, 4, 5\};$$

$$A_{420}(j \rightarrow k) = A_{420}(k \rightarrow j) = 0 \quad j \in \{1, 2\} \quad k \in \{3, 4, 5\};$$

$$A_{500}(j \rightarrow k) = \delta_{jk} \quad j, k \in \{1, 2, 3\}; \quad A_{500}(j \rightarrow k) = 1 - \delta_{jk} \quad j, k \in \{4, 5\};$$

$$A_{500}(j \rightarrow k) = \delta_{jk} \quad j, k \in \{6, 7, 8\}; \quad A_{500}(j \rightarrow k) = A_{500}(k \rightarrow j) = 0$$

$$j \in \{1, 2, 3\} \quad k \in \{4, 5, 6, 7, 8\};$$

$$A_{500}(j \rightarrow k) = A_{500}(k \rightarrow j) = 0 \quad j \in \{4, 5\} \quad k \in \{6, 7, 8\};$$

$$A_{600}(j \rightarrow k) = \delta_{jk} \quad j, k \in \{1, 2, 3, 4\};$$

$$A_{600}(j \rightarrow k) = 1 - \delta_{jk} \quad j, k \in \{5, 6\};$$

$$A_{600}(j \rightarrow k) = A_{600}(k \rightarrow j) = 0 \quad j \in \{1, 2, 3, 4\} \quad k \in \{5, 6\};$$

representing 56 configurations giving collisions: 20 identical to model I with or without rest particles as "spectator", 24 two-body collisions changing the number of rest particles of mass one with or without rest particles of mass two as "spectator", and 12 two-body collisions exchanging the number of rest particles of mass one and two. The viscosities are given by

$$\nu = \frac{1}{28d(1-d)^3(1 - \frac{4d}{7}(1 - \frac{d(1-d)}{d^2+(1-d)^2}))} - \frac{1}{8}$$

$$\zeta = \frac{2c_s^4}{d(1-d)^4} \left(\frac{1}{16} \left(\frac{1}{c_s^2} - \frac{5}{3} \right)^2 + \frac{1}{9} \frac{d(1-d)}{(d^2 + (1-d)^2)^3} \right) - \frac{1}{2} \left(\frac{1}{2} - c_s^2 \right). \quad (2.15)$$

3. Computer simulations

The present work was done by simulation of the lattice gas models on an FPS-164 using lattices of order 10^6 nodes with a typical speed of 10^6 updates per second [5-8]. The evolution of the lattice gas is computed according to a parallel iteration in five steps.

1. The states of the nodes of obstacles and boundaries are saved in a temporary storage.
2. During this second step, the collision step, the new state of each node is computed as a function of its old state according to the collision rules.
3. The third step is used to determine the new states of the nodes of obstacles and boundaries which are computed as a function of the saved states and the collision rules on obstacles.
4. During the fourth step, the propagation step, the bits of states of each node are propagated toward one of the neighbor nodes according to the physical interpretation of the different bits.
5. This last step is used to set the lattice boundary conditions.

All the programs were written in FORTRAN, using a few tricks to take advantage of the architecture of the computer. Since these tricks are introduced to make the best use of a pipeline architecture, they can be used for most of the vectorized machines and thus will be described in some detail.

3.1 Boundary conditions on the lattice edges and on the obstacles

The basic boundary conditions on the lattice edges can be periodic in the two directions; the particles exiting from one edge are reinjected into the other edge in the same direction. In what follows, we refer to this case as periodic boundary condition.

Another situation, related to a wind-tunnel experiment, consists in providing a flux of fresh particles on one side of the lattice and allowing an output flux on the other side.⁵ The exact distribution of input and output particles is derived from equation (2.5) with an appropriate density and velocity. The balance between the input and output fluxes leads to an adjustment of the average speed of the flow inside the "wind tunnel", which depends upon the presence of lateral boundaries or obstacles.

Obstacles are first decomposed into a series of continuous links which approximate its geometrical shape. At nodes which represent an obstacle, particles are either bounced back ($c_i \rightarrow -c_i$) or can be reflected by the boundary of the obstacle. The first case corresponds to a very strict "no-slip" condition, whereas the second case is more closely related to the "slip" condition. One could also diffuse the particles by re-emitting them at random on available links, but that would be more complicated to implement. Momentum transfer between the gas and the obstacle can be computed during step one, leading to forces experienced by the obstacle.

For the present, triangular lattice of the FHP lattice gas, the natural way to label nodes uses nonorthonormal coordinates so that lattices are diamonds. As this is awkward for most situations, we have used lattices whose shape is rectangular. This can be implemented by taking different propagation rules for lines of odd or even parity. On even lines, directions 2 and 6 imply a change of the horizontal coordinate, whereas on odd lines, directions 3 and 5 are associated with a change of the horizontal coordinate. This is displayed in figure 1. This feature complicates only very slightly the computer program corresponding to step 4 of the simulation. However, when a specialized hardware is designed, provision must be made for different propagation rules on odd and even lines as is done in the RAP-1 machine [9]. When working with rectangular physical space, the number of nodes has to be multiplied by $\frac{\sqrt{3}}{2}$ to measure lengths along the vertical axis.

3.2 Collision and propagation steps

During the second step, the post-collision state is computed using either a look-up table or the appropriate combination of Boolean operators. In the case of a look-up table, the states are coded with eight bits (one byte)

⁵ More precisely, in order to keep the density almost constant, particles are also injected on the output side along the links directed toward the inside of the lattice. The physical meaning of these boundary conditions remains to be clarified.

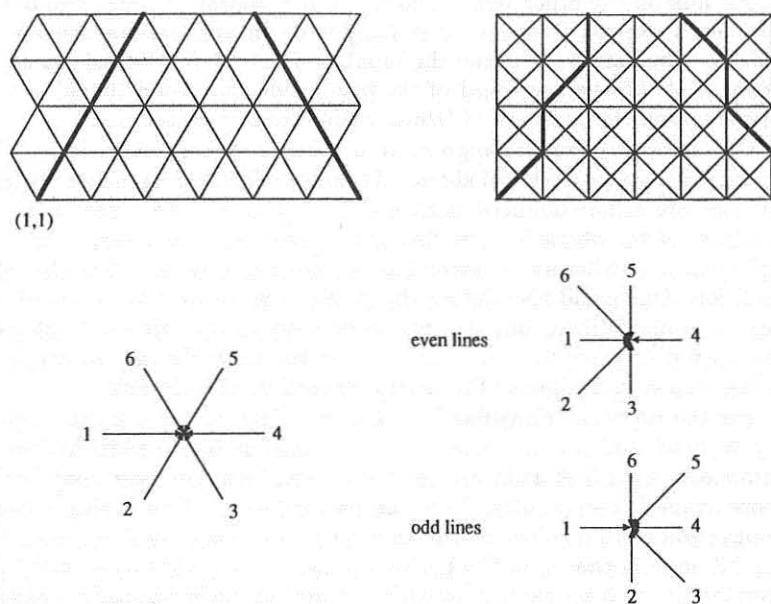


Figure 1: Schematic representation of the six velocity directions and of the lattice used in the FHP lattice gas: Left with 60° angles, Right adapted to orthonormal coordinates.

and eight nodes are packed in each of the 64-bit words of the FPS. During the collision step, the bytes are extracted from the word and used as an address to fetch their new value stored in a look-up table computed once at the beginning of the program. For the six- or seven-bit models, the eighth bit is used as a "random" bit to obtain probabilities $1/2$ when it is needed. This bit is initially set at random with an average density $1/2$ and is complemented each time a collision occurs. For the eight-bit models, two different look-up tables are used for the odd and even iterations of the whole lattice. It was checked on the seven-bit models that this procedure does not significantly bias the results. During the propagation step, the bits coding the different particles are extracted from the word using masks and moved as a whole, thus saving computation steps.

When Boolean operators are used to code the collision rules, 64 nodes are packed in a word and six to eight words are used to code the different particles. The noninteger probabilities of transition are implemented using a new collision rule at each iteration of the lattice. The minimum number of Boolean operators⁶ needed to implement models I to III are given in Appendix B along with the basic tools we used to obtain good results with a reasonable amount of work. The propagation step is obtained by the motion of a full word; thus, during the collision and the propagation steps, 64 nodes are computed simultaneously, allowing high computation speed to be reached. The use of the Boolean rules needs more work than that of the look-up table to obtain efficient codes, but is more suited to pipeline or vector computers; thus, we used the first solution for the mature programs, while the latter was used for preliminary investigations of the various models.

3.3 Initialization and measurements

Initial flows were generated by Monte-Carlo procedure with average population N_{ik} related to the local density and velocity by equation (2.5). The use of the linear expansion restricts the available speeds to $\frac{\rho_m}{2\rho}$, greater values giving negative or greater-than-one probabilities which will introduce initial conditions far from equilibrium. Note that we do not take into account the corrections of the equilibrium distributions with the gradients of the density and velocity fields, since they require the knowledge of the viscosities and are considered along with the nonlinear terms as corrections to the leading orders. Macroscopic quantities are obtained by averaging the N_{ik} according to equation (2.1) over rectangular regions with shapes and sizes adapted to the flow under study. For nonlinear flow simulations, we always used the momentum instead of the velocity, since the momentum is

⁶We have used only the Boolean operators available on a general purpose computer: and, or, exclusive-or, and complement. More compact rules can certainly be obtained on computers with more Boolean operators as the Connection Machine [10]. In addition, minimum must be taken as the lowest number of operators we found; some operators may probably be saved working harder than we did.




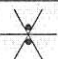



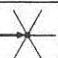
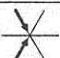
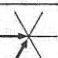
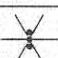
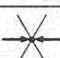
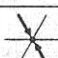
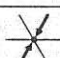
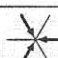
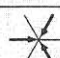
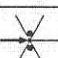

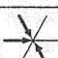
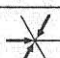
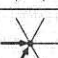
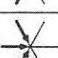
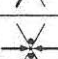
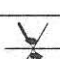
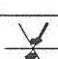
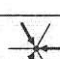
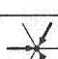
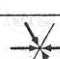
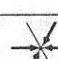
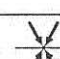
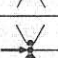
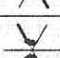
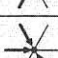
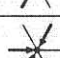
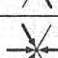
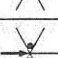
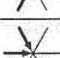

| n | jx | jy | | folds |
|---|----|----|---|-------|
| 0 | 0 | 0 |  | 1 |
| 1 | 0 | 0 |  | 1 |
| 1 | 2 | 0 |  | 6 |
| 2 | 0 | 0 |     | 1 |
| 2 | 2 | 0 |   | 6 |
| 2 | 3 | 2 |  | 6 |
| 3 | 0 | 0 |       | 1 |
| 3 | 2 | 0 |     | 6 |
| 3 | 3 | 2 |  | 6 |
| 3 | 4 | 0 |  | 6 |
| 4 | 0 | 0 |         | 1 |
| 4 | 2 | 0 |      | 6 |
| 4 | 3 | 2 |   | 6 |
| 4 | 4 | 0 |  | 6 |

Table 3: List of configurations for the eight-bit model. Configurations with five particles and more are obtained by duality replacing particles by holes and holes by particles.

the relevant variable in the incompressible steady cases [3,11]. Moreover, it naturally comes out of the simulations.

4. Equilibrium distributions

Theoretically, the equilibrium distributions of the local averaged densities N_{ik} in direction i are given by Fermi-Dirac functions depending upon the density ρ and the average velocity \mathbf{u} . This property was checked by the simulation of the time evolution of a 512×256 lattice with periodic boundary conditions in both directions. The first 24 time steps were discarded to remove the transient behavior. We checked that this number of time steps was larger than the duration of the transient. We then measured the average populations for each direction averaged on the next eight time steps. These simulations were done on model II for densities per moving cell 0.2 and 0.5 for velocities from $-6/7\sqrt{3}$ to $6/7\sqrt{3}$ and for velocities along the bisector of two \mathbf{c}_i . In this case, the average densities of rest particles and particles moving in the directions perpendicular to the velocity are equal. The densities of particles moving on symmetric directions are also equal; thus, there are only three independent unknowns which can be obtained exactly from the solution of a third-degree equation [12]. Figure 2 shows the equilibrium distributions as a function of the velocity for the different populations along with the theoretical curves obtained from the exact solution. These distributions were normalized by the average population at rest. Clearly, the results of the simulations agree very well with the predicted Fermi-Dirac distributions with an error smaller than one percent. Note that for $d = 0.5$, the nonlinearity vanishes due to the Fermi-Dirac distributions and the particular orientation of the velocity with respect to the lattice.

Another test was performed with model IV in which the population of rest particles of mass two depends upon the population of moving particles in a nonlinear way, given by equation (2.3). Figure 3 shows the variation of d_1 as a function of d together with its value obtained by simulations.

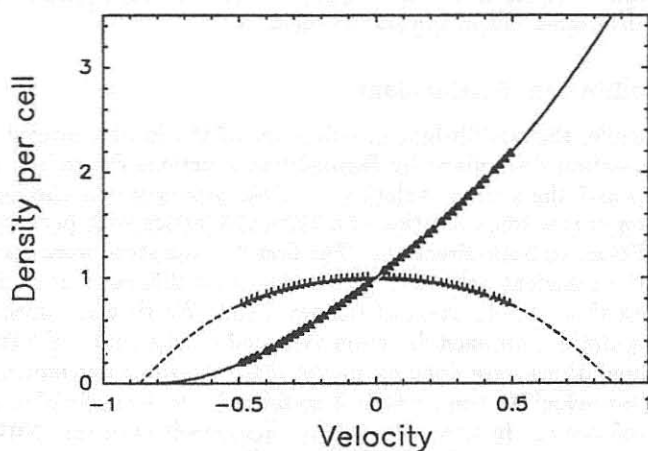
5. Linear hydrodynamics

The velocity of sound c_s and the kinematic shear and bulk viscosities ν and ζ of the lattice gas models described above have been measured using the relaxation of an initial periodic perturbation $\mathbf{u}(\mathbf{r}, 0)$ of the velocity field [13]: $\mathbf{u}(\mathbf{r}, 0) = (\mathbf{u}_{\parallel} + \mathbf{u}_{\perp}) \cos(\mathbf{k} \cdot \mathbf{r})$, where \mathbf{k} is the wave vector of the perturbation and \mathbf{u}_{\parallel} and \mathbf{u}_{\perp} are the velocity components parallel and perpendicular to the wave vector [14].

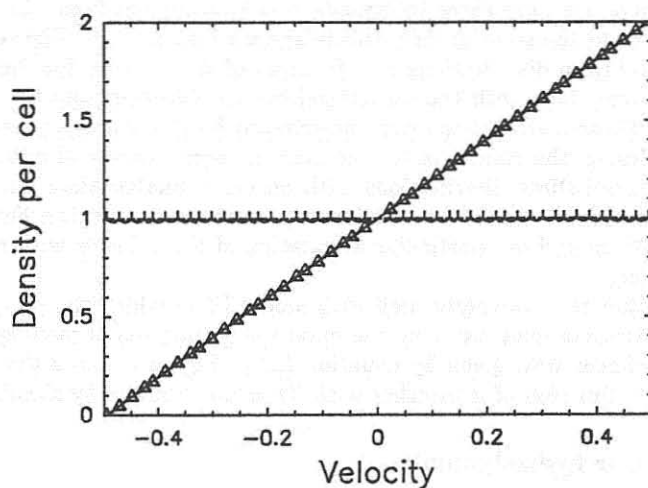
The relaxation in time of the velocity $\mathbf{u}(\mathbf{r}, t)$ and of the density perturbation $\delta\rho(\mathbf{r}, t)$ are given by

$$\mathbf{u}(\mathbf{r}, t) =$$

$$(\mathbf{u}_{\parallel} \cos(\omega t + \varphi) \exp(-k^2(\nu + \zeta)t/2) + \mathbf{u}_{\perp} \exp(-k^2\nu t)) \cos(\mathbf{k} \cdot \mathbf{r}), \quad (5.1)$$



a



b

Figure 2: Variation of the density N_i versus velocity. Closed triangles correspond to angle 60° between \mathbf{u} and \mathbf{c}_i , apex correspond to angle 90° between \mathbf{u} and \mathbf{c}_i . Solid lines are obtained theoretically (a) at a mean density of 0.2, (b) at a mean density of 0.5.

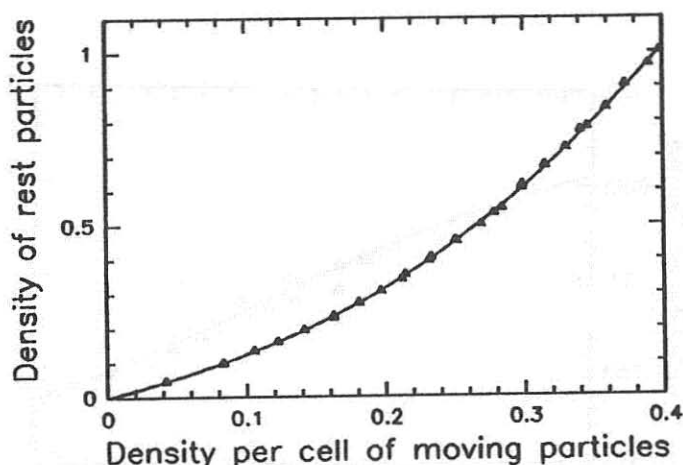


Figure 3: Comparison of theoretical and measured values of the density of rest particles versus density of moving particles for the eight-bit model.

$$\delta\rho(\mathbf{r}, t) = (\rho u_{\parallel}/c) \sin(\omega t) \exp(-k^2(\nu + \zeta)t/2) \sin(\mathbf{k} \cdot \mathbf{r}), \quad (5.2)$$

with $\omega = c_s k$, $\tan \varphi = k(\nu + \zeta)/2c_s$.

Starting from the initial conditions, at each time step, the momentum and the density are averaged along lines perpendicular to the wave vector. The result is Fourier transformed to get the components of the momentum and density corresponding to k . From the relaxation curves, c_s , ν , and ζ are measured by least squares fits of equations (5.1) and (5.2) to the time evolution of $u_{\perp}(k)$, $u_{\parallel}(k)$, and $\rho(k)$.

The measured sound velocities are isotropic and agree with theoretical values $1/\sqrt{2}$ for model I and $\sqrt{3/7}$ for models II and III. Figure 4 shows the dependence of the speed of sound with the density per cell for the eight-bit model, compared to the theoretical given by equation (2.14). The measured values of the viscosities are summarized in figures 5a to d, along with the theoretical curves computed from equations (2.10), (2.12), (2.13), and (2.15). These measurements were obtained on 256×512 lattices with periodic boundary conditions and for wavelength between 30 and 80 nodes, with no observable effects of the wave numbers on the viscosities over a factor ten on the relaxation times. The size of the symbols corresponds roughly to the error bars. Without rest particles, the experimental values of ν are above the theoretical curve for the measurements corresponding to sound waves, while those corresponding to shear waves are below. Thus, the kinematic bulk viscosity ζ is found negative, which is an unphysical result. At present, no convincing explanation has been found for this effect, which may be related to the fact that there are few triple symmetric

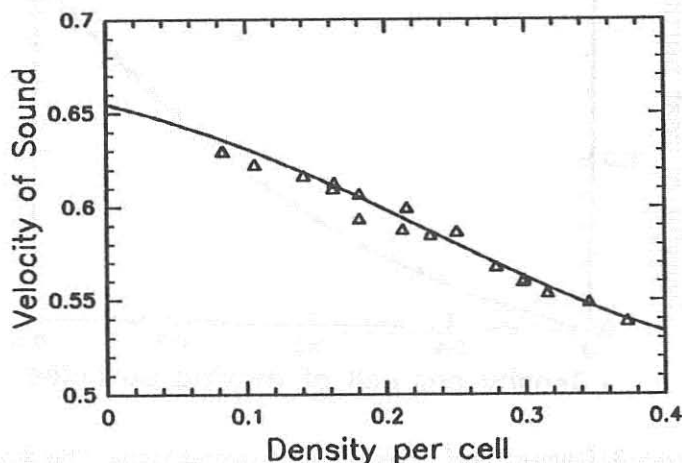


Figure 4: Theoretical and experimental values of the speed of sound for the eight-bit model.

collisions needed to remove a spurious invariant, leading to very long relaxation times of the associated microscopic quantity in comparison with the hydrodynamics time scales. The measured viscosities agree with theoretical predictions for models II, III, and IV. Thus, the presence of rest particles apparently improves the behavior of the lattice gas while decreasing the viscosity significantly, leading to higher Reynolds numbers [15]. Moreover, these results show that the Boltzmann approximation is well verified, even for high densities.

In many simulations, we have considered several disturbances at the same time, taking as initial conditions:

$$\sum_{i=1}^3 (u_{i\parallel} \cos \mathbf{k}_i \mathbf{r} + u_{i\perp} \cos \mathbf{k}_i \mathbf{r}) \quad (5.3)$$

and found essentially no coupling between these various waves. Furthermore, we found that the acoustic properties are particularly insensitive to the amplitude of waves.

A uniform motion of the fluid, at speed u , advects sound or shear waves at speed $g(\rho)u$, as discussed in reference 16.

6. Nonlinear flow simulations

We now present a few examples of flows computed by the lattice gas method. These flows were chosen in order to perform quantitative com-

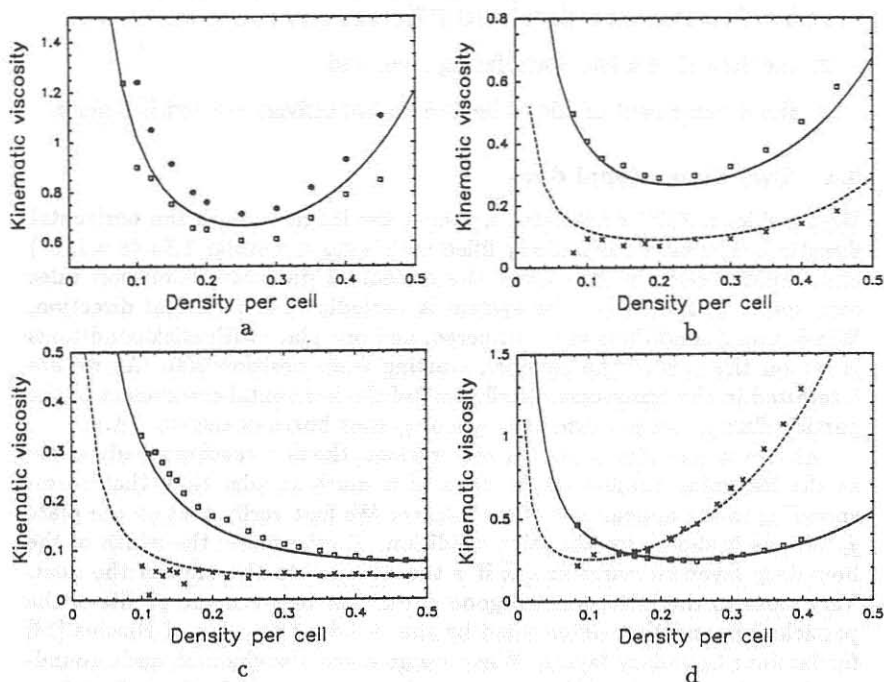


Figure 5: Theoretical shear (solid lines) and bulk (dashed lines) reduced viscosities as a function of the reduced density, compared with the results of numerical simulations for different lattice gas models: (a) original FHP model, (b) model II with rest particles and limited collision rules, (c) model III with rest particles and all possible collisions, and (d) eight-bit model IV.

parisons with results obtained either in real experiments or using standard solutions of the Navier-Stokes equations. Three problems are considered here:

1. the formation of boundary layers and the development of a Poiseuille flow in a two-dimensional duct [17],
2. the flow after a backward facing step, and
3. the development of eddies behind an impulsively started flat plate.

6.1 Two-dimensional duct

We consider a 3072×512 lattice, taking the longer side as the horizontal direction. The lattice is initially filled with a gas of density 1.54 ($d = 0.22$) and uniform velocity 0.30 along the horizontal direction. Collision rules correspond to model II. The system is periodic in the vertical direction. Wind-tunnel conditions are considered, and one plate with stick conditions is set on the axis of the channel, starting from position 300. As we are interested in the transverse distribution of the horizontal component of the particle flux j_x , we perform averages of j_x over boxes of size 48×1 .

After a large enough number of iterations, the flow reaches steady state, as the Reynolds number in the channel is much smaller than that corresponding to the appearance of turbulence. We first verify that on the plate $j_x = 0$, as it should for the stick condition. Furthermore, the width of the boundary layer increases as \sqrt{x} if x the distance to the inlet of the duct. Very close to the inlet, we find good agreement between the profile of the particle flux and that determined by the standard solution of Blasius [18] for laminar boundary layers. When we go down the channel, each boundary layer is affected by the presence of the other and leads at first to a compression of the boundary layers and eventually to the formation of a parabolic profile, known as Poiseuille flow.

The complete description of such an experimental situation has been performed by Slichting [19]. We have followed his solution by calculating the profile of the flow versus distance to the inlet of the duct using an iterative method to solve the Navier-Stokes equations. The velocity of the incoming fluid is measured in the steady-state regime, and the viscosity is measured in a separate experiment performed at the same density; thus, there is no adjustable parameter for the comparison of theory and experimental data obtained with the lattice gas. Figure 6 shows successive profiles of the horizontal component of the particle flux for different values of the relative distance to the inlet of the duct $z = x/w$. Very good agreement between theory and experiment is obtained provided one uses $\nu_{\text{eff}} = \nu/g(\rho)$.

6.2 Backward facing step

Another well-known flow situation is that of a two-dimensional backward facing step at low Reynolds number. This situation was considered as a

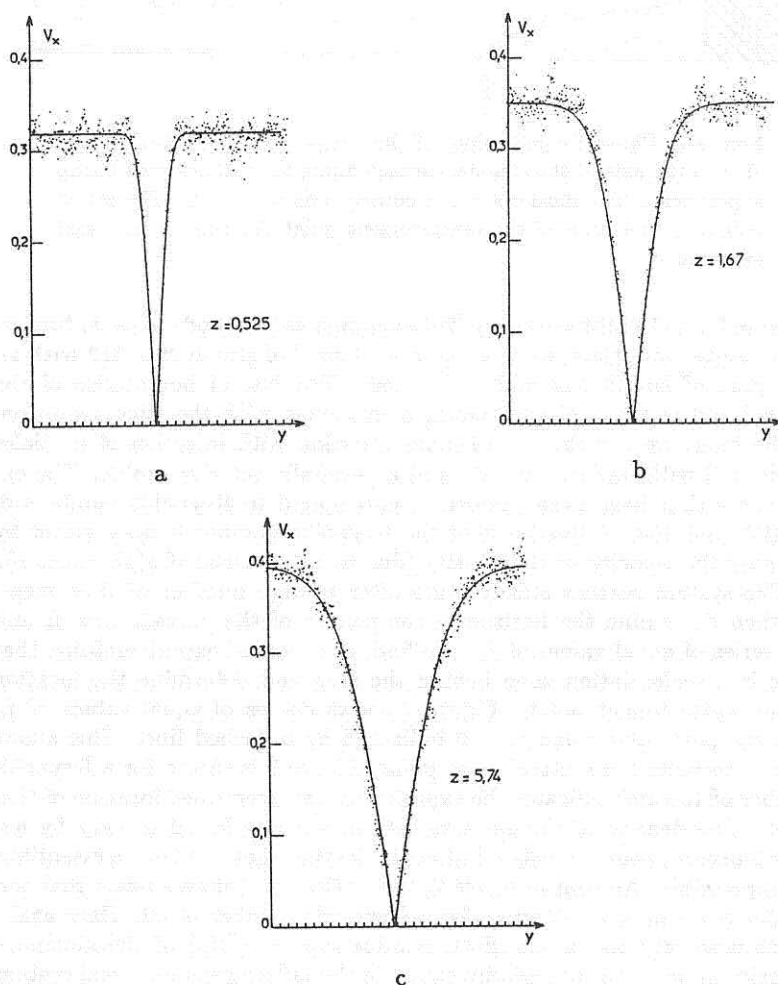


Figure 6: Velocity component parallel to a plate set in the middle of a channel at relative distance from the apex of the plate (a) 0.525, (b) 1.67, and (c) 5.74. The dots are obtained by the lattice gas simulations; the solid lines are calculated using the Slichting method.

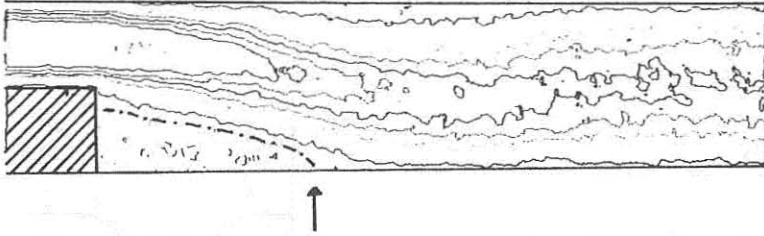


Figure 7: Plots of equal values of the component of the flux j_x parallel to the axis of the channel corresponding to the backward facing experiment. The dash-dot curve corresponds to $j_x = 0$. The arrow points the location of the reattachment point determined in a real experiment.

test case for a GAMM workshop [20] on numerical methods to solve Navier-Stokes equations. Here, we have used a channel of size 4608×512 with an inlet part of length 512 and width 256. The lateral boundaries of the channel and of the backward facing step are set with the stick condition. At the inlet, we use the wind-tunnel situation with injection of particles distributed with uniform density and a parabolic velocity profile. The experiments that have been performed correspond to Reynolds numbers of 50, 100, and 150. Adjustment of the Reynolds number is done either by changing the velocity or the density (due to dependence of $g(\rho)$ versus ρ).

The system reaches steady state after a large number of time steps. We then determine the horizontal component of the particle flux j_x and plot series of equal values of j_x . We find, as observed experimentally, that there is a recirculation zone behind the step and determine the location of the reattachment point. Figure 7 shows curves of equal values of j_x , with the particular value $j_x = 0$ indicated by a dashed line. This allows us to determine the reattachment point. Figure 7 is shown for a Reynolds number of 150 and indicates the experimentally determined location of that point. The density of the gas was determined and found to vary by less than 3 percent over the entire lattice, indicating that the flow is essentially incompressible. As seen in figure 7, the lattice gas behaves like a real one. Similar agreement is obtained for a Reynolds number of 50. Here again, it was necessary to use an effective value $\nu_{\text{eff}} = \nu/g(\rho)$ of the kinematic viscosity in order to successfully compare the lattice gas and a real system.

6.3 Impulsively started flat plate

This is the simplest case of interaction of a lattice gas flow with an obstacle. Here, we consider a 2816×1024 lattice with periodic conditions along y and the wind-tunnel condition at the left and right edges. Initially, the lattice is filled with a gas of uniform density and speed. Here we take $d = 0.30$, ($\rho = 2.1$), and $v = 0.428$. The collision rules correspond to model III, so that the Mach number is 0.654 and the effective Reynolds number is

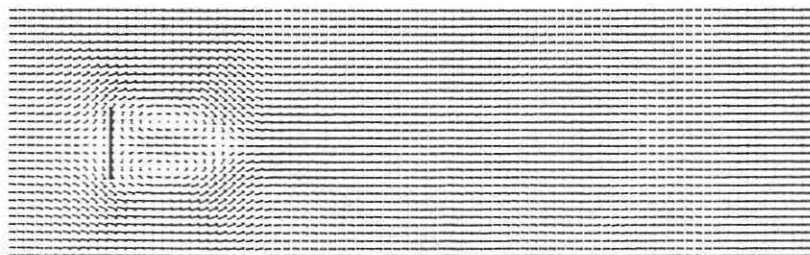


Figure 8: Map of the flux of particles in a 886.8×2048 channel 3000 time steps after the introduction of a flat plate of real size 216.5. The distance between the back of the plate and the point where $j_x = 0$ on the axis of the channel is defined as the size of the wake.

approximatively 300. The value of d is close to that of the minimum of the effective kinematic viscosity $\nu_{\text{eff}} = \nu/g(\rho)$, so that small compressibility effects should not be important.

Now, at $t = 0$, we insert a flat plate of real width $w = 216.5$ perpendicular to the input flow. It is set with stick conditions. The presence of the plate first produces shock waves due to the reflection of particles at the surface of the plate, then eddies start to develop symmetrically on either edges of the plate, as shown in figure 8.

Here, we present detailed data concerning the location of the wake, defined as the point where the horizontal component of the particle flux j_x is 0 for the symmetry axis of the problem. If s is the distance from this point to the plate, we consider the relative size of the wake s/w . We then measure s/w as a function of a reduced time $\theta = vt/w$, where v is the incoming velocity and t the real time. This choice of variables corresponds to that used in the analysis of real experiments performed in water by Taneda and Honji [21]. These authors found that

$$s/w = 0.89(vt/w)^{2/3}$$

independently of the Reynolds number Re , when $18 < \text{Re} < 1100$.

We show in figure 9 the “experimental” value of s/w determined for the lattice gas flow versus $(vt/w)^{2/3}$ for a Mach number equal to 0.327 ($v = 0.214$). We find a linear relationship, with a slope of 0.46.

To compare our value of the slope to that of a real experiment, we have again to consider that a lattice gas follows the Navier-Stokes equation, provided the velocity is multiplied by a factor $g(\rho)$. This means we have to compare the slope measured with the lattice gas (0.46) with a renormalized slope $0.89g^{2/3} = 0.423$ in the present case.

Again, we reach almost quantitative agreement between a lattice gas flow and a real experiment, provided we use a properly renormalized value of the velocity.

When time reaches sufficiently large values, it is found that the symmetry of the flow is broken and vortex shedding by the plate occurs. This

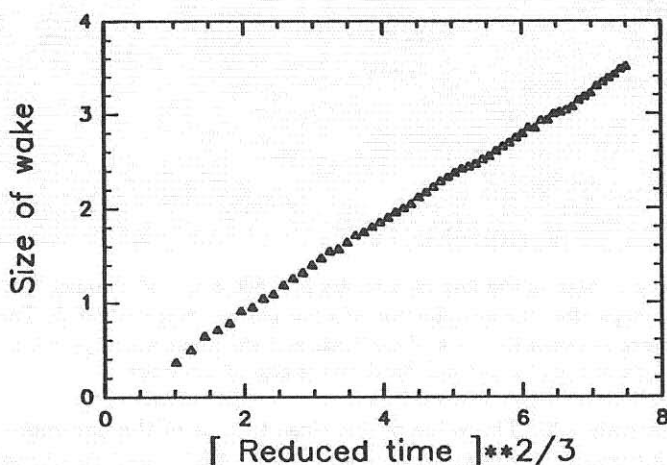


Figure 9: Relative size of the wake behind an impulsively started flat plate s/w as a function of $(vt/w)^{2/3}$.

leads to the formation of a two-dimensional Von Karman street, an example of which is shown in figure 10.

In another experiment, performed at a larger input speed, we have determined the period of the vortex shedding. The value corresponds to a Strouhal number of approximately 0.20, to be compared to a measured value of 0.16 for a truly incompressible flow at roughly the same Reynolds number.

Detailed comparisons between lattice gas flows and real flows like those presented here should be performed at higher velocities to find out which effects are produced by a breakdown of the incompressibility conditions.

7. Conclusion

Quantitative agreement between theory and simulation has been demonstrated in both the linear and nonlinear regimes for moderate Reynolds numbers, provided a properly renormalized value of the fluid velocity ($v \rightarrow g(\rho)v$) is used in the nonlinear advection term of the Navier-Stokes equation. It should be noted that the introduction of obstacles into the flow is particularly simple and represents, for the cases studied, a computational overhead of a few percent. The present models are limited to Reynolds numbers of order of 10^3 and incompressible flows. Moreover, since local equilibrium is a function of ρ and ρu only, such models cannot simulate thermal phenomena. However, more complicated models derived from the FHP model [22–24] may overcome most of these limitations in a near future. In this case, lattice gas simulations will be a new tool for experimental work

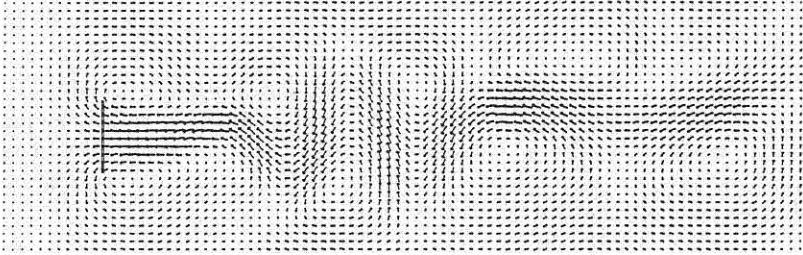


Figure 10: Similar to figure 8, but after 40000 iterations showing the formation of a Karman street. To emphasize the vortices, the mean momentum has been subtracted from the local ones.

in hydrodynamics, with the main advantage of being inherently stable.

Acknowledgments

We thank U. Frisch, B. Hasslacher, M. Hénon, Y. Pomeau, Y. H. Qian, and J. P. Rivet for helpful discussions; A. Noullez for participation in some of the simulations; and GRECO 70 "Expérimentation numérique" for support.

Appendix A. Boltzmann approximation with rest particles

In this appendix, we will indicate how the theoretical results of reference 2 must be modified to handle the cases with particles with zero velocity and different masses. These modifications will be given for the Boltzmann approximation only.

The macroscopic quantities density, ρ , and momentum, $\rho \mathbf{u}$, are related to the local average populations N_{ik} of particles with mass m_k and velocity \mathbf{c}_i , by

$$\rho = \sum_{i,k} m_k N_{ik}; \quad \rho \mathbf{u} = \sum_{i,k} m_k N_{ik} \mathbf{c}_i. \quad (\text{A.1})$$

The demonstration used in Appendix C of reference 3 proves that, at equilibrium and for uniform density and velocity, $\{\log(N_{ik}) - \log(1 - N_{ik})\}$ is a collision invariant if the collisions verify the semi-detailed balance. The conclusion is now

$$N_{ik} = \frac{1}{1 + \exp(m_k(h + \mathbf{q} \cdot \mathbf{c}_i))}, \quad (\text{A.2})$$

where h and \mathbf{q} are nonlinear functions of ρ and \mathbf{u} . When $\mathbf{u} = 0$, the average density is the same for all the particles with same mass m_k and will be denoted d_k . Taking the mass of the lightest particles as unit mass and $d_0 = d$, one gets

$$d_k = \frac{d^{m_k}}{d^{m_k} + (1-d)^{m_k}} \quad (\text{A.3})$$

The general expansion of the Fermi-Dirac distributions around small u is quite complicated, and we will restrict it to the case of b_m moving particles with unit mass and velocity c and b_r rest particles with mass $m_k = 2^k, k \in \{0, \dots, b_r - 1\}$. The density of moving and rest particles, ρ_m and ρ_r respectively, can be defined as

$$\rho_m = b_m d \quad \text{and} \quad \rho_r = \sum_{k=0}^{b_r-1} m_k d_k, \quad \text{with} \quad \rho = \rho_m + \rho_r \quad (\text{A.4})$$

Let

$$c_s^2 = \frac{b_m d(1-d)c^2}{D(b_m d(1-d) + \sum_{k=0}^{b_r-1} m_k^2 d_k(1-d_k))} \quad (\text{A.5})$$

For small u , the expansion of equation (A.2) up to second order gives in D dimensions:

$$N_{i0}^{eq} = d \left(1 + \frac{D}{c^2} \frac{\rho}{\rho_m} c_i \cdot u + G(\rho) (Q_{i\alpha\beta} + \left(\frac{c^2}{D} - c_s^2 \right) \delta_{\alpha\beta}) u_\alpha u_\beta \right)$$

$$N_{0k}^{eq} = d_k \left(1 - m_k c_s^2 G(\rho) \frac{1-d_k}{1-d} \delta_{\alpha\beta} u_\alpha u_\beta \right) \quad (\text{A.6})$$

where

$$Q_{i\alpha\beta} = \begin{cases} c_{i\alpha} c_{i\beta} - \frac{c^2}{D} \delta_{\alpha\beta} & \text{if } i \neq 0 \\ 0 & \text{if } i = 0 \end{cases},$$

$$\text{and} \quad G(\rho) = \frac{D^2}{2c^4} \frac{\rho^2}{\rho_m^2} \frac{(1-2d)}{(1-d)}. \quad (\text{A.7})$$

When there are density and velocity gradients, this equilibrium distribution is modified by first-order correction in gradients:

$$N_{i0}^{(1)} = (\psi Q_{i\alpha\beta} - X \delta_{\alpha\beta}) \partial_{1\alpha} (\rho u_\beta) = \psi Q_{i\alpha\beta} \partial_{1\alpha} (\rho u_\beta) + X \delta_{\alpha\beta} \partial_{i1} \rho$$

$$N_{0k}^{(1)} = \chi_k \delta_{\alpha\beta} \partial_{1\alpha} (\rho u_\beta) = -\chi_k \delta_{\alpha\beta} \partial_{i1} \rho \quad (\text{A.8})$$

where

$$X = \frac{1}{b_m} \sum_{k=0}^{b_r-1} m_k \chi_k \quad (\text{A.9})$$

Using the same Chapman-Enskog expansion as in references 2, 3, and 25 up to second-order terms in velocity and gradients, one gets

$$\begin{aligned}
\partial_t \rho + \operatorname{div}(\rho \mathbf{u}) &= 0 \\
\partial_t(\rho u_\alpha) + \partial_\beta(g(\rho)\rho u_\alpha u_\beta) &= \\
&- \partial_\alpha P(\rho, u^2) + \partial_\beta(\nu \partial_\beta(\rho u_\alpha)) + \partial_\alpha\left(\left(\frac{D-2}{D}\nu + \zeta\right)\operatorname{div}(\rho \mathbf{u})\right), \quad (\text{A.10})
\end{aligned}$$

with

$$\begin{aligned}
g(\rho) &= \frac{D}{D+2} \frac{\rho}{\rho_m} \frac{1-2d}{1-d}, \\
P(\rho, u^2) &= \frac{\rho_m}{D} c^2 - \rho g(\rho) \frac{c_s^2}{c^2} \left(1 + \frac{D}{2} - \frac{c^2}{2c_s^2}\right) u^2 \quad (\text{A.11})
\end{aligned}$$

and where the kinematic shear and bulk viscosities, ν and ζ , are given by

$$\nu = -\frac{b_m c^4}{D(D+2)} \psi - \frac{c^2}{D(D+2)}; \quad \zeta = \frac{b_m c^2}{D} X - \frac{1}{2} \left(\frac{c^2}{D} - c_s^2\right) \quad (\text{A.12})$$

and the speed of sound is c_s , since:

$$\left(\frac{\partial P}{\partial \rho}\right)_{u=0} = \frac{b_m d(1-d)c^2}{D(b_m d(1-d) + \sum_{k=0}^{b_r-1} m_k^2 d_k(1-d_k))} = c_s^2. \quad (\text{A.13})$$

Since the density is no longer linearly related to the density per cell d , the perturbation $N_{ik}^{(1)}$ must be taken as $d_k(1-d_k)N_{ik}^{*(1)}$,

$$\begin{aligned}
\psi &= d(1-d)\psi^*, \\
\chi_k &= d_k(1-d_k)\chi_k^*, \\
X &= d(1-d)X^* \quad (\text{A.14})
\end{aligned}$$

and, in the Boltzmann approximation, $N_I^{*(1)}$ is related to N_I^{eq} by

$$\partial_{t_1} N_I^{eq} + c_{i\alpha} \partial_{1\alpha} N_I^{eq} = \sum_J \mathcal{A}_{IJ}^* N_J^{*(1)} \quad (\text{A.15})$$

where the linearized collision matrix is given by

$$\mathcal{A}_{IJ}^* = -\frac{1}{2} \sum_{ss'} (s_I - s'_I)(s_J - s'_J) A(s \rightarrow s') \prod_K d_K^{s_K} (1-d_K)^{1-s_K} \quad (\text{A.16})$$

It is more convenient to rewrite the matrix $[\mathcal{A}_{IJ}^*]$ as

$$[\mathcal{A}_{IJ}^*] = \begin{pmatrix} [\mathcal{R}_{kl}] & [\mathcal{C}_{kj}] \\ [\widetilde{\mathcal{C}}_{il}] & [\mathcal{M}_{ij}] \end{pmatrix} \quad (\text{A.17})$$

where $[\mathcal{R}_{kl}]$ and $[M_{ij}]$ are square submatrices with respectively b_r and b_m rows, $[C_{kj}]$ is a submatrix with b_r rows of b_m identical columns $[C_k]$, and $[\tilde{C}_{il}]$ is the transposed of $[C_{kj}]$. Since $[m_I]$ is an eigenvector of $[A_{IJ}^*]$ with a zero eigenvalue, one must have

$$\begin{aligned} b_m C_k + \sum_l m_l \mathcal{R}_{kl} &= 0 \quad \forall k \\ \sum_l m_l C_l + \sum_j M_{ij} &= 0 \quad \forall i \end{aligned} \quad (\text{A.18})$$

Then, ψ^* and χ_k^* are obtained by the solubility condition of the following linear system:

$$\begin{aligned} \frac{Dc_s^2}{b_m c^2} m_k \frac{d_k(1-d_k)}{d(1-d)} \partial_{t_1} \rho &= (b_m C_k X^* - \sum_l \mathcal{R}_{kl} \chi_l^*) \partial_{t_1} \rho \\ \frac{D}{b_m c^2} \left((c_s^2 - \frac{c^2}{D}) \partial_{t_1} \rho + Q_{i\alpha\beta} \partial_{1\alpha} (\rho u_\beta) \right) &= - \sum_l (C_l (m_l X^* + \chi_l^*)) \partial_{t_1} \rho \\ &\quad + \sum_j M_{ij} Q_{j\alpha\beta} \psi^* \partial_{1\alpha} (\rho u_\beta) \end{aligned} \quad (\text{A.19})$$

Using equation (A.18), this condition gives

$$\frac{Dc_s^2}{b_m c^2} m_k \frac{d_k(1-d_k)}{d(1-d)} = (b_m C_k X^* - \sum_l \mathcal{R}_{kl} \chi_k^*), \quad (\text{A.20})$$

$$\frac{D}{b_m c^2} Q_{i\alpha\beta} = \sum_j M_{ij} Q_{j\alpha\beta} \psi^*. \quad (\text{A.21})$$

Thus, ψ^* is simply related to the eigenvalue λ of the linearized collision matrix A_{IJ}^* corresponding to the eigenvector $[c_{ix} c_{iy}]$:

$$\psi^* = \frac{D}{b_m c^2} \frac{1}{\lambda} \quad (\text{A.22})$$

but the χ_k^* are given by the solution of the linear system of b_r equations given by equation (A.20). We will only sketch how the values of ζ were obtained for equations (2.12), (2.13), and (2.15).

The following results are valid when $m_k = 2^k$ and when the collisions are such that they change the total mass of rest particles only by one mass unit. In this case, the submatrix $[\mathcal{R}_{kl}]$ and C_k can be written

$$\begin{aligned}
 [\mathcal{R}_{kl}] &= b_m \sum_{n=0}^{b_r-1} a_n [\mathcal{R}_{kl}^{(n)}] \\
 c_k &= a_k - \sum_{n=k+1}^{b_r-1} a_n
 \end{aligned} \tag{A.23}$$

with:

$$[\mathcal{R}_{kl}^{(n)}] = \begin{pmatrix} \overbrace{0 \ \cdots \ 0}^{b_r-n-1 \text{ times}} & 0 & \overbrace{0 \ \cdots \ 0}^{n \text{ times}} \\ \vdots & \ddots & \vdots \\ 0 & \cdots & 0 \\ 0 & \cdots & 0 \\ 0 & \cdots & 0 \\ \vdots & \ddots & \vdots \\ 0 & \cdots & 0 \end{pmatrix} \begin{pmatrix} 0 \\ \vdots \\ 0 \\ -1 \\ 1 \\ \vdots \\ 1 \end{pmatrix} \begin{pmatrix} 0 & \cdots & 0 \\ 0 & \cdots & 0 \\ 0 & \cdots & 0 \\ 1 & -1 & \cdots & -1 \\ -1 & 1 & \cdots & -1 \\ \vdots & \vdots & \ddots & \vdots \\ -1 & -1 & \cdots & -1 \end{pmatrix} \tag{A.24}$$

Equation (A.20) becomes

$$\begin{aligned}
 \frac{Dc_s^2}{b_m c^2} m_k \frac{d_k(1-d_k)}{d(1-d)} &= b_m \left(X^* + \chi_k^* - \sum_{l=0}^{k-1} \chi_l^* \right) a_k \\
 &- b_m \sum_{n=k+1}^{b_r-1} \left(X^* + \chi_n^* - \sum_{l=0}^{n-1} \chi_l^* \right) a_n
 \end{aligned} \tag{A.25}$$

since the solution of the linear system

$$Y_k - \sum_{l=0}^{k-1} Y_l = A_k$$

is given by

$$Y_k = \frac{1}{2} (A_k + \sum_{l=0}^k 2^{k-l} A_l).$$

Equation (A.25) gives:

$$\chi_k^* - \sum_{l=0}^{k-1} \chi_l^* = \frac{Dc_s^2}{2b_m c^2} \frac{E_k}{m_k a_k} - X^* \tag{A.26}$$

with

$$E_k = \frac{1}{b_m} \left(m_k^2 \frac{d_k(1-d_k)}{d(1-d)} + \sum_{l=k}^{b_r-1} m_l^2 \frac{d_l(1-d_l)}{d(1-d)} \right), \tag{A.27}$$

then

$$\chi_k^* = \frac{Dc_s^2}{4b_m c^2} \left(\frac{E_k}{m_k a_k} + \sum_{l=0}^k 2^{k-l} \frac{E_l}{m_l a_l} \right) - m_k X^* \quad (\text{A.28})$$

$$X^* = \frac{D^2 c_s^4}{4b_m c^4} \sum_{k=0}^{b_r-1} \frac{E_k^2}{a_k m_k^2} \quad (\text{A.29})$$

and, finally,

$$\zeta = d(1-d) \frac{Dc_s^4}{4c^2} \left(\frac{1}{a_0} \left(\frac{c^2}{Dc_s^2} - 1 + \frac{1}{b_m} \right)^2 + \sum_{k=1}^{b_r-1} \frac{E_k^2}{a_k m_k^2} \right) - \frac{1}{2} \left(\frac{c^2}{D} - c_s^2 \right). \quad (\text{A.30})$$

Thus, for $D = 2$, $c^2 = 1$, $b_m = 6$, and $b_r = 1$ and 2, equation (A.30) respectively gives

$$\zeta = \frac{d(1-d)}{98a_0} - \frac{1}{28}, \quad (\text{A.31})$$

and

$$\zeta = d(1-d) c_s^4 \left(\frac{1}{16a_0} \left(\frac{1}{c_s^2} - \frac{5}{3} \right)^2 + \frac{1}{9a_1} \frac{d_1^2(1-d_1)^2}{d^2(1-d)^2} \right) - \frac{1}{2} \left(\frac{1}{2} - c_s^2 \right). \quad (\text{A.32})$$

Appendix B. Boolean laws

The basic concept used to look for minimal set of Boolean functions to implement the collision rules is a derivation of the algorithm used by Hardy, de Pazzis, and Pomeau [26] for the four-bit model on a square lattice. A basic collision operator can be written

$$c = a_1 \cdot \bar{a}_2 \cdot a_3 \cdot \bar{a}_4 + \bar{a}_1 \cdot a_2 \cdot \bar{a}_3 \cdot a_4 = (a_1 \oplus a_2) \cdot (a_2 \oplus a_3) \cdot (a_3 \oplus a_4) \quad (\text{B.1})$$

where $a \cdot b$, $a + b$, $a \oplus b$, and \bar{b} correspond respectively to the *and*, *or*, *exclusive-or*, and *not* operators. The new states are then obtained by

$$a_i = c \oplus a_i. \quad (\text{B.2})$$

The computation of the new configuration needs only nine Boolean operators. This basic algorithm can be extended to the triangular case by the definition of several collision operators. Each collision exchanges at least two particles and two holes, when this exchange does not change the total momentum; thus, we can define four-bit collisions operators similar to the one given in equation (B.1).

Appendix B.1 Model I

In this model, the basic collision operators give the possibility of head-on collisions γ_i and of triple symmetric collisions δ :

$$\begin{aligned} t_i &= a_i \oplus a_{i+1} \quad i = \{1, \dots, 6\} \\ u_i &= t_i \cdot t_{i+3} \quad i = \{1, 2, 3\} \\ \gamma_i &= u_i \cdot (a_{i+1} \oplus a_{i+3}) \quad i = \{1, 2, 3\} \\ \delta &= u_1 \cdot u_2 \cdot u_3 \end{aligned} \quad (\text{B.3})$$

Note that these operators are unchanged by duality, and for two- or four-body collisions, two of them are non-zero. Thus, for a model with all the possible collisions, the collision operators must choose between the different possible collisions using two different sets of collision operators:

$$c_i = \delta + \gamma_i + \gamma_{i+2} \cdot \bar{\gamma}_{i+1}, \quad i = \{1, 2, 3\} \quad (\text{B.4})$$

or

$$c_i = \delta + \gamma_{i+2} + \gamma_i \cdot \bar{\gamma}_{i+1}, \quad i = \{1, 2, 3\} \quad (\text{B.5})$$

and the new configuration is given by

$$\begin{aligned} a_i &= c_i \oplus a_i, \\ a_{i+3} &= c_i \oplus a_{i+3}, \\ i &= \{1, 2, 3\} \end{aligned} \quad (\text{B.6})$$

for a total of 35 elementary Boolean operators.

For model I, the collision operators defined in equation (B.4) must be modified to allow collisions only for two-body configurations. This requires checking the absence of particles in the two directions not used to define the γ_i :

$$c_i = \delta + \gamma_i \cdot \overline{(a_{i+2} + a_{i+5})}, \quad i = \{1, 2, 3\} \quad (\text{B.7})$$

or

$$c_i = \delta + \gamma_{i+2} \cdot \overline{(a_{i+1} + a_{i+4})}, \quad i = \{1, 2, 3\} \quad (\text{B.8})$$

The algorithm to compute the collision step for model I, uses equations (B.3), (B.7) or (B.8) and (B.6), for a total of 35 elementary operators.

Appendix B.2 Model III

The algorithm for the model III can be easily derived for the algorithm for the six-bit model with all the possible collisions. A new step must be added to equation (B.3) to handle the case of rest particles:

$$\epsilon_i = t_i \cdot t_{i+5} \cdot (a_0 \oplus a_{i+1}) \quad i = \{1, \dots, 6\} \quad (\text{B.9})$$

The choice between two possible collisions is now done by the collision operator c_0 of the rest particles:

$$\begin{aligned} c_0 &= \overline{\delta + (\gamma_1 + (\epsilon_1 \oplus \bar{\epsilon}_4)) \cdot (\gamma_2 + (\epsilon_2 \oplus \bar{\epsilon}_5)) \cdot (\gamma_3 + (\epsilon_3 \oplus \bar{\epsilon}_6))}, \\ c_i &= \delta + \bar{c}_0 \cdot (\gamma_i + \gamma_{i+2} \cdot \bar{\gamma}_{i+1}) + c_0 \cdot (\epsilon_{i+5} + \epsilon_i \cdot \bar{\epsilon}_{i+2} + \epsilon_{i+1} \cdot \bar{\epsilon}_{i+3}) \\ &\quad i = \{1, 2, 3\}, \\ c_{i+3} &= \delta + \bar{c}_0 \cdot (\gamma_i + \gamma_{i+2} \cdot \bar{\gamma}_{i+1}) + c_0 \cdot (\epsilon_{i+2} + \epsilon_{i+3} \cdot \bar{\epsilon}_{i+5} + \epsilon_{i+4} \cdot \bar{\epsilon}_i) \\ &\quad i = \{1, 2, 3\} \end{aligned} \quad (\text{B.10})$$

or

$$\begin{aligned} c_0 &= \overline{\delta + (\gamma_1 + (\epsilon_2 \oplus \bar{\epsilon}_5)) \cdot (\gamma_2 + (\epsilon_3 \oplus \bar{\epsilon}_6)) \cdot (\gamma_3 + (\epsilon_1 \oplus \bar{\epsilon}_4))}, \\ c_i &= \delta + \bar{c}_0 \cdot (\gamma_{i+2} + \gamma_i \cdot \bar{\gamma}_{i+1}) + c_0 \cdot (\epsilon_{i+1} + \epsilon_i \cdot \bar{\epsilon}_{i+4} + \epsilon_{i+5} \cdot \bar{\epsilon}_{i+3}) \\ &\quad i = \{1, 2, 3\}, \\ c_{i+3} &= \delta + \bar{c}_0 \cdot (\gamma_{i+2} + \gamma_i \cdot \bar{\gamma}_{i+1}) + c_0 \cdot (\epsilon_{i+4} + \epsilon_{i+3} \cdot \bar{\epsilon}_{i+1} + \epsilon_{i+2} \cdot \bar{\epsilon}_i) \\ &\quad i = \{1, 2, 3\}. \end{aligned} \quad (\text{B.11})$$

The new configurations are computed using equation (B.5) and

$$a_0 = c_0 \oplus a_0. \quad (\text{B.12})$$

Thus, the algorithm for the model III uses equations (B.3), (B.9), (B.10), or (B.11), (B.6), and (B.12), for a total of 103 elementary Boolean operators,⁷ if $\bar{\epsilon}_i$, $\epsilon_i \cdot \bar{\epsilon}_{i+4}$ and $\delta + \bar{c}_0 \cdot (\gamma_i + \gamma_{i+2} \cdot \bar{\gamma}_{i+1})$ are computed only once.

Appendix B.3 Model II

The algorithm for the model II is slightly different of the previous one, since many possible configurations must be removed.

$$\begin{aligned} t_i &= a_i \oplus a_{i+1}, \quad u_i = t_i \cdot \bar{a}_{i+4} \quad i = \{1, \dots, 6\} \\ v_i &= (t_i \cdot t_{i+3}) \cdot u_{i+1} \cdot u_{i+4} \quad i = \{1, 2, 3\} \end{aligned} \quad (\text{B.13})$$

The choice between head-on collisions is done by

⁷Two additional operators can be saved in equation (B.9) using $a_0 \oplus a_2$ for $i = 1, 3$ and $a_0 \oplus a_3$ for $i = 2, 4$.

$$\gamma_i = v_i + v_{i+1}, \quad i = \{1, 2, 3\} \quad (\text{B.14})$$

or

$$\gamma_i = v_i + v_{i+2}, \quad i = \{1, 2, 3\} \quad (\text{B.15})$$

and δ is computed using only two *and* operators (the quantities inside parentheses being computed during (B.13) step) by

$$\begin{aligned} \delta &= (t_1 \cdot t_4) \cdot (t_2 \cdot t_5) \cdot (t_3 \cdot t_6) \\ \epsilon_i &= t_i \cdot t_{i+5} \cdot (a_0 \oplus a_{i+1}) \cdot \bar{a}_{i+2} \quad i = \{1, \dots, 6\} \end{aligned} \quad (\text{B.16})$$

The collision operators c_i are given by

$$\begin{aligned} c_0 &= \epsilon_1 + \epsilon_2 + \epsilon_3 + \epsilon_4 + \epsilon_5 + \epsilon_6 \\ c_i &= (\delta + \gamma_i) + \epsilon_i + \epsilon_{i+1} + \epsilon_{i+5} \quad i = \{1, 2, 3\} \\ c_{i+3} &= (\delta + \gamma_i) + \epsilon_{i+3} + \epsilon_{i+4} + \epsilon_{i+2} \quad i = \{1, 2, 3\} \end{aligned} \quad (\text{B.17})$$

The new configurations are computed using equations (B.6) and (B.12). Thus, the algorithm for the model II uses equations (B.13), (B.14), or (B.15), (B.16), (B.17), (B.6), and (B.12), for a total of 82 elementary Boolean operators, if some or operations are computed only once in equation (B.17).

References

- [1] U. Frisch, B. Hasslacher and Y. Pomeau, *Phys. Rev. Lett.*, **56** (1986) 1505.
- [2] U. Frisch, D. d'Humières, B. Hasslacher, P. Lallemand, Y. Pomeau and J. P. Rivet, *Complex Systems*, **1** (1987) 646. (This paper lists most of the relevant references in the field of lattice gases.)
- [3] U. Frisch and J.P. Rivet, *C. R. Acad. Sci. Paris XII*, **303** (1986) 1065.
- [4] M. Hénon, "Calcul de la viscosité dans le réseau triangulaire" and "Viscosité d'un réseau", preprints, Observatoire de Nice, B.P.139, 06003 Nice Cedex, France.
- [5] D. d'Humières, Y. Pomeau and P. Lallemand, *C. R. Acad. Sci. Paris XII*, **301** (1985) 1391.
- [6] D. d'Humières, P. Lallemand and T. Shimomura, "An experimental study of lattice gas hydrodynamics", *Los Alamos preprint*, LA-UR-85-4051 (1985).
- [7] D. d'Humières, Y. Pomeau and P. Lallemand, *Innovative Numerical Methods in Engineering*, (A Computational Mechanics Publication, Springer-Verlag, Berlin, 1986) 241.

- [8] D. d'Humières and P. Lallemand, *C. R. Acad. Sci. Paris XII*, **302** (1985) 983.
- [9] A. Clouqueur and D. d'Humières, "RAP1, a cellular automaton machine for fluid dynamics", *Complex Systems*, **1** (1987) 584.
- [10] S. Hillis, "The Connection machine", (M.I.T. Press, Cambridge, MA, 1986).
- [11] D. Levermore, private communication.
- [12] G. Doolen, private communication.
- [13] R. D. Mountain, *Rev. of Mod. Physics*, **38** (1966) 205.
- [14] Other methods can be used to measure ν ; see, for example, F. Hayot, "Viscosity in lattice gas automata", *Physica D*, (1987), in press, or L. Kadanoff, G. MacNamara, and G. Zanetti, "Size-dependence of the shear viscosity for a two-dimensional lattice gas", University of Chicago preprint (1987).
- [15] D. d'Humières and P. Lallemand, *Physica*, **140A** (1986) 326.
- [16] D. d'Humières, P. Lallemand and G. Searby, "Numerical Experiments on Lattice Gases: Mixtures and Galilean Invariance", *Complex Systems*, **1** (1987) 632.
- [17] D. d'Humières and P. Lallemand, *C. R. Acad. Sci. Paris XII*, **302** (1985) 983.
- [18] H. Slichting, *Boundary layer theory*, (Pergamon Press, London, 1955).
- [19] H. Slichting, *Z.A.M.M.*, **14** (1934) 368.
- [20] GAMM workshop, in *Note on Numerical Fluid Mechanics*, **9**, K. Morgan, J. Périaux and F. Thomasset, eds. (Vieweg and Sons, 1984).
- [21] S. Taneda and H. Honji, *J. Phys. Soc. Japan*, **30** (1971) 262.
- [22] C. Burges and S. Zaleski, *Complex Systems*, **1** (1987) 31.
- [23] P. Clavin, D. d'Humières, P. Lallemand and Y. Pomeau, *C. R. Acad. Sci. Paris*, **303** (1986) 1169.
- [24] P. Clavin, P. Lallemand, Y. Pomeau and G. Searby, *J. Fluid Mech.*, in press.
- [25] S. Wolfram, *J. of Stat. Phys.*, **45** (1986) 471.
- [26] J. Hardy, O. de Pazzis and Y. Pomeau, *Phys. Rev.*, **A13** (1976) 1949.